JOURNAL OF GEOPHYSICAL RESEARCH, VOL. 112, C07031, doi:10.1029/2006JC003655, 2007

Biological response to circulation driven by mean summertime winds off central Chile: A numerical model study

Mark E. Baird,[1] Ole Leth,[2,3] and John F. Middleton[4,5]

Received 18 April 2006; revised 4 April 2007; accepted 8 May 2007; published 28 July 2007.

[1] A coupled physical-biological model of the waters off central Chile is used to investigate the nitrogen-phytoplankton-zooplankton response to ocean circulation driven by mean summertime winds. The circulation drives the upwelling of middepth water onto the continental shelf and reaches a quasistable rate between days 40 and 60 of the simulation. High-nutrient, low-phytoplankton biomass water is upwelled at the coast, with nutrients being converted to phytoplankton within 3–10 days. A lagged response in zooplankton occurs after 6–30 days, by which time the water has been advected offshore. The magnitude and spatial distribution of phytoplankton biomass and export of organic matter off the continental shelf is sensitive to the zooplankton mortality term. For low zooplankton mortality, phytoplankton biomass on the continental shelf is limited by grazing pressure due to zooplankton, phytoplankton and zooplankton biomass remains low, and the nitrogen advected off the continental shelf in the surface waters is primarily dissolved inorganic nitrogen. When the mortality rate is increased fourfold, an approximately fourfold to fivefold increase is seen in the continental shelf phytoplankton biomass, phytoplankton productivity, and export of organic matter to the deep ocean. This dependence on zooplankton mortality illustrates the potential of top-down control of the shelf production and export of organic matter off the central Chile continental shelf.

Citation: Baird, M. E., O. Leth, and J. F. Middleton (2007), Biological response to circulation driven by mean summertime winds off central Chile: A numerical model study, *J. Geophys. Res.*, *112*, C07031, doi:10.1029/2006JC003655.

1. Introduction

[2] The ecosystem off the coast of central Chile is one of the most productive in the world. Rates of depth-averaged primary productivity vary seasonally, with monthly averages between 0.5 and 6.1 g C m^{-2} d^{-1} [*Daneri et al.*, 2000], and daily values ranging from 0.3–9.6 g C m^{-2} d^{-1} [*Cuevas et al.*, 2004; *Fossing et al.*, 1995]. The primary productivity of the region can support up to 4% of the world's annual fish landings [*Daneri et al.*, 2000].

[3] The extremely high productivity of the Chilean coastal waters is attributable to upwelling of nutrient-rich Peru-Chile undercurrent waters, and processes that maintain populations in the shallow coastal waters [*Atkinson et al.*, 2002]. In particular, the dominance of alongshore currents when compared to cross shelf currents provides sufficient residence times for a range of biological processes. The physical circulation along the central Chilean coast has been modeled using the sigma coordinate, primitive equation, Princeton Ocean Model [*Mesias et al.*, 2003; *Leth and Shaffer*, 2001; *Leth and Middleton*, 2004]. These studies emphasize the importance wind-driven circulation and the presence of eddies in driving coastal upwelling.

[4] The trophic web of the upwelling system off central Chile has been modeled using the Ecopath and Ecosim approach [*Neira and Arancibia*, 2004]. Among the findings of this study was that the typical trophic level of the fishery was 2.97, and was representative of small to medium sized pelagic fish. Approximately 15% of the primary productivity is required to sustain the local fisheries landing [*Neira and Arancibia*, 2004]. While these findings emphasize the importance of high primary productivity in determining fish stocks, the approach used is unable to resolve the spatial and temporal links between physical processes such as upwelling and biological processes that make the central Chilean waters so productive.

[5] A coupled physical-biological model is used to understand the biological implications of circulation driven by the mean summertime winds off Chile. The effects of circulation on the dynamics of dissolved inorganic nitrogen (DIN), phytoplankton and zooplankton biomass are inves-

[1]Climate and Environmental Dynamics Laboratory, School of Mathematics and Statistics, University of New South Wales, Sydney, New South Wales, Australia.
[2]Department of Geophysics, University of Concepción, Concepción, Chile.
[3]Now at Centre for Ocean and Ice, Danish Meteorological Institute, Copenhagen, Denmark.
[4]Aquatic Sciences, South Australian Research and Development Institute, West Beach, South Australia, Australia.
[5]Climate and Environmental Dynamics Laboratory, School of Mathematics and Statistics, University of New South Wales, Sydney, New South Wales, Australia.

0148-0227/07/2006JC003655$09.00

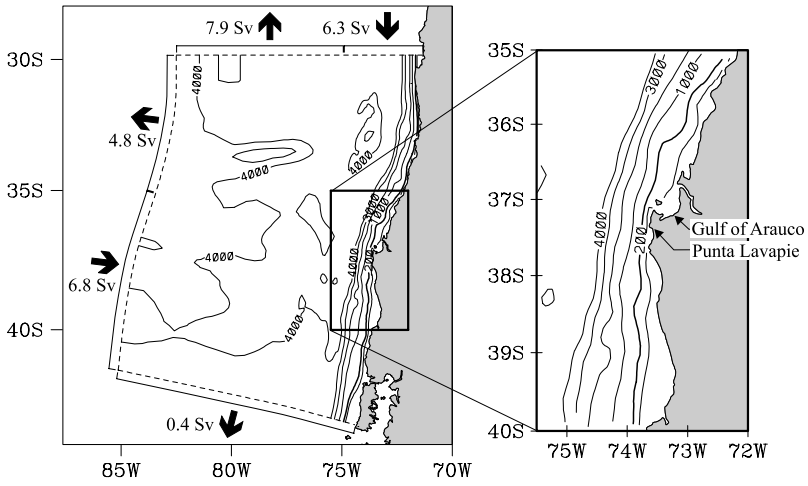

Figure 1. Model topography. Isobath depths are in meters. The arrows near the edge of the domain indicate the net transports that are specified in the open boundary conditions.

tigated, as well as the fluxes of organic matter between the continental shelf and deeper waters. Simulations of the coupled model at three values of the zooplankton mortality coefficient are used to illustrate the sensitivity of the system to top-down control. Finally, a diagnostic tracer age is used to investigate the relationship between physical forcings and the timing of the biological processes.

2. Model Description

2.1. Physical Model

[6] The physical model is the Princeton Ocean Model (POM) which has a free surface and solves the nonlinear primitive equations on a horizontal orthogonal curvilinear grid and a vertical sigma (terrain following) coordinate system using finite difference methods [*Blumberg and Mellor*, 1987]. Turbulence parameters are calculated using the *Mellor and Yamada* [1982] second-order turbulence closure scheme.

[7] The physical configuration used is similar to that of *Leth and Middleton* [2004]. The model domain is about 1000 km in the offshore direction and 1500 km in the alongshore direction (Figure 1). The cross-shore grid spacing is about 2 km over the continental shelf and slope, increasing to 25 km at the western boundary. The alongshore grid spacing is approximately 15 km.

[8] Differences between the physical configuration used here and that of *Leth and Middleton* [2004] are: (1) the number of vertical sigma layers has been increased to 36 to better resolve the surface mixed layer, with the thickness of the top 9 layers being 0.48, 0.48, 0.48, 0.48, 0.48, 0.72, 1.44, 1.92 and 2.88% of the total depth. Layers 10 through to 22 have a thickness of 3.85% of the total depth, and 3 layers resolve the bottom boundary layer as in the original configuration [*Leth and Middleton*, 2004]; (2) the advection scheme has been changed from the original POM centered difference scheme to a positive definite advection scheme [*Smolarkiewicz*, 1984] with 3 iterations to improve the representation of advection, and avoid negative values for the biological tracers; and (3) the Craig-Banner scheme [*Craig and Banner*, 1994] for calculating the wave-driven flux of turbulent kinetic energy at the surface has been implemented. Using this surface flux, the *Mellor and Yamada* [1982] turbulence closure scheme produces a more realistic near surface vertical profile of the dissipation rate of turbulent kinetic energy (which is used by the biological model to calculate grazing rates).

[9] The model is forced with a summertime climatology based on weekly European Remote Sensing Satellite scatterometer wind stress estimates averaged from December to February for the years 1991 to 2000 (Figure 2). Open ocean boundaries are specified from the output of the Ocean Circulation and Climate Advanced Modelling Project (OCCAM) model (Figure 1). The initial conditions for temperature and salinity are derived from the World Ocean Atlas [*Levitus and Boyer*, 1994; *Levitus et al.*, 1994]. For

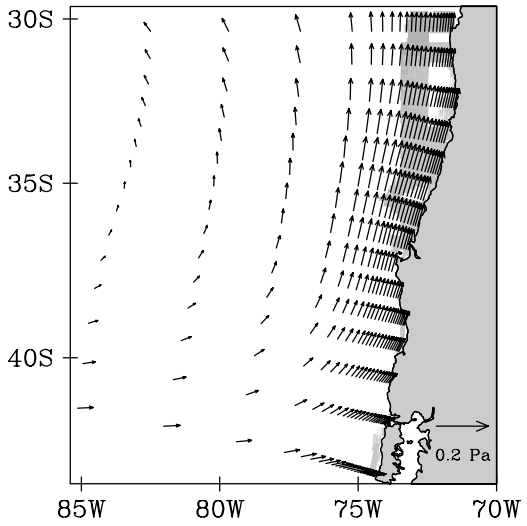

Figure 2. Mean summertime (December–February) wind stress for 1991–2000. The shaded region corresponds to a cyclonic (upwelling favorable) wind stress curl.

further details of the physical model configuration and physical forcing, see *Leth and Middleton* [2004].

2.2. Biological Model

[10] The NPZ model used is the pelagic ecosystem model of *Baird et al.* [2004]. The model includes the processes of nutrient uptake and light capture by phytoplankton, phytoplankton growth from internal reserves, zooplankton grazing on phytoplankton, and the mortality and sinking of both phytoplankton and zooplankton. Where possible, physical descriptions of the limits to ecological processes have been used. For example, the description of grazing rates of zooplankton on phytoplankton incorporates an encounter rate calculation, based on the encounter rates of particles in a turbulent fluid, which places a maximum rate on ingestion and therefore of zooplankton growth. The physical limits are used up until a physiological rate, such as maximum growth rate, becomes more limiting.

[11] The model contains 5 state variables: dissolved inorganic nitrogen, or DIN, (N), phytoplankton (P), zooplankton (Z), and phytoplankton reserves of nitrogen (R_N) and energy (R_I). For comparison, a commonly used alternate term for quantifying nitrogen reserves is total algal nitrogen or the cell quota, Q_N [mol N cell^{-1}], which is given by $Q_N = m_{P,N} + R_N$, where $m_{P,N}$ is the stoichiometry coefficient of nitrogen in phytoplankton, and represents the minimum quantity of nitrogen for which a cell remains viable. The calculation of $m_{P,I}$, the stoichiometry coefficient of energy, is based on the quantum yield of photosynthesis and the Redfield ratio (C:N = 106:16 [*Redfield et al.*, 1963]). The theoretical maximum quantum yield is 0.125 mol C (mol photon)$^{-1}$. A more realistic value of 0.1 mol C (mol photon)$^{-1}$ has been used [*Kirk*, 1994].

[12] The coupling of the physical and biological models results in an advection-diffusion-reaction (ADR) equation for phytoplankton biomass with the following dynamical terms:

$$\frac{\partial P}{\partial t} + \mathbf{v}\cdot\nabla P = \nabla\cdot(K\nabla P) + F_P - w_P\frac{\partial P}{\partial z}, \tag{1}$$

where the symbol $\nabla = (\frac{\partial}{\partial x}, \frac{\partial}{\partial y}, \frac{\partial}{\partial z})$, $\mathbf{v}$ is the velocity field, K is the eddy diffusion coefficient, and varies in space and time, F_P is the sink/sources of phytoplankton due to biological processes and w_P is the sinking velocity of phytoplankton. The ADR equations for DIN, zooplankton and reserves of nitrogen and energy are given in a two-dimensional form in equations (12)–(16) of *Baird et al.* [2004], and can be extended to three dimensions following equation (1). Note that while these equations are written in a z-coordinate system, they are solved in the sigma coordinates of the model grid.

[13] The equations for the sink/sources of DIN, phytoplankton, zooplankton, nitrogen and energy reserves are given by

$$F_N = -k_N\left(\frac{R_N^{\max}-R_N}{R_N^{\max}}\right)\frac{P}{m_{P,N}} + \zeta_P P + \zeta_P R_N\frac{P}{m_{P,N}} + \zeta_Z Z + \gamma\min\cdot\left[\phi P/m_{P,N}, \frac{\mu_Z^{\max}}{(1-\gamma)}\right]Z + \min\left[\phi P/m_{P,N}, \frac{\mu_Z^{\max}}{(1-\gamma)}\right]Z\frac{R_N}{R_N^{\max}}, \tag{2}$$

$$F_{R_N} = +k_N\left(\frac{R_N^{\max}-R_N}{R_N^{\max}}\right) - \mu_P^{\max}\left(m_{P,N}+R_N\right)\frac{R_N}{R_N^{\max}}\frac{R_I}{R_I^{\max}}, \tag{3}$$

$$F_{R_I} = +k_I\left(\frac{R_I^{\max}-R_I}{R_I^{\max}}\right) - \mu_P^{\max}\left(m_{P,I}+R_I\right)\frac{R_N}{R_N^{\max}}\frac{R_I}{R_I^{\max}}, \tag{4}$$

$$F_P = +\mu_P^{\max}\frac{R_N}{R_N^{\max}}\frac{R_I}{R_I^{\max}}P - \min\left[\phi P/m_{P,N}, \frac{\mu_Z^{\max}}{(1-\gamma)}\right]Z - \zeta_P P, \tag{5}$$

$$F_Z = +\min\left[\phi P/m_{P,N}, \frac{\mu_Z^{\max}}{(1-\gamma)}\right]Z - \gamma\min\left[\phi P/m_{P,N}, \frac{\mu_Z^{\max}}{(1-\gamma)}\right]Z - \zeta_Z Z, \tag{6}$$

where k_N and k_I are the maximum rates of DIN and energy uptake of phytoplankton respectively (and are a function of N and incident light respectively), $R_N^{\max}$ and $R_I^{\max}$ are the maximum values of R_N and R_I respectively, $\mu_P^{\max}$ and $\mu_Z^{\max}$ are the maximum growth rates of phytoplankton and zooplankton respectively, ϕ is the encounter rate coefficient between phytoplankton and zooplankton, ζ_P and ζ_Z are the linear mortality rates of phytoplankton and zooplankton respectively, and $(1-\gamma)$ is the assimilation efficiency of grazing by zooplankton on phytoplankton. The sink/source terms F_N, F_P and F_Z have units of mol N m^{-3} s^{-1}, while F_{R_N} has units of mol N cell^{-1} s^{-1}, and F_{R_I} has units of mol photon cell^{-1} s^{-1}. The term $P/m_{P,N}$ which appears in the DIN uptake and the phytoplankton grazing terms, is the concentration of phytoplankton cells [cell m^{-3}].

[14] The encounter rate calculations are based on the curvilinear formulations of *Jackson* [1995] and include the effect of the size of the predator and prey on encounters. This is quantified as the encounter rate coefficient, ϕ, which is given by the sum of encounters due to diffusion, $\phi_{diffusion}$, relative velocity (due to swimming and sinking), $\phi_{rel.vel.}$, and turbulent shear, ϕ_{shear},

$$\phi = \phi_{diffusion} + \phi_{rel.vel.} + \phi_{shear}, \tag{7}$$

where $\phi_{diffusion} = (2\ k_B T/3\eta)\ (1/r_{prey} + 1/r_{pred})\ (r_{prey} + r_{pred})$, $\phi_{rel.vel.} = 0.5\ \pi r_{prey}^2\ U$, and $\phi_{shear} = 9.8\frac{p^2}{(1+2p)^2}\ (\frac{\varepsilon}{\nu})^{0.5}\ (r_{prey} + r_{pred})^3$. The variables r_{pred} and r_{prey} are the radii of the predator and prey, and $p = \frac{r_{prey}}{r_{pred}}$, $r_{pred} > r_{prey}$. The symbol ν is the kinematic viscosity, η is the dynamic viscosity, $k_B = 1.38 \times 10^{-23}$ J K^{-1} is the Boltzmann constant, U is the relative encounter velocity and ε is the rate of dissipation of turbulent kinetic energy. The phytoplankton concentration at which zooplankton grazing switches from being limited by encounters between predators and prey to being limited by the maximum zooplankton growth rate is $P = \mu_Z^{\max}\ m_{P,N}/((1-\gamma)\phi) \sim$ 0.4 mmol N m^{-3} for low values of small-scale turbulence, and decreases as shear increases.

[15] A more detailed description of the biological model is given by *Baird et al.* [2004], and its application to the

Table 1. Parameter Values Used in the Simulations[a]

Parameter	Symbol	Value	Units
		Model Parameters	
P equivalent spherical radius	r_P	1	μm
Z equivalent spherical radius	r_Z	20	μm
Assimilation coefficient	γ	0.3	-
P linear mortality	ζ_P	0.0	d^{-1}
Z linear mortality	ζ_Z	0.5 μ_Z^{max}, 0.25 μ_Z^{max}, 0.125 μ_Z^{max}	d^{-1}
		Parameters Calculated From r_P and r_Z	
P nitrogen content	$m_{P,N}$	1.34×10^{-14}	mol N $cell^{-1}$
P energy content	$m_{P,I}$	8.87×10^{-13}	mol I $cell^{-1}$
Maximum P N reserves	R_N^{max}	1.34×10^{-14}	mol N $cell^{-1}$
Maximum P energy reserves	R_I^{max}	8.87×10^{-13}	mol I $cell^{-1}$
Z nitrogen content	$m_{Z,N}$	1.22×10^{-11}	mol N $cell^{-1}$
Diffusion shape factor	ψ	1.26×10^{-5}	m $cell^{-1}$
P Chl concentration	C	1.35×10^{7}	mg Chl m^{-3}
Absorption cross section	$\overline{aA}$	2.17×10^{-13}	m^2 $cell^{-1}$
P Chl:N ratio	CV/m_N	4.21	$\frac{\text{mg Chl } a}{(\text{mmol N})^{-1}}$
Maximum growth rate of P	μ_P^{max}	2.82	d^{-1}
Maximum growth rate of Z	μ_Z^{max}	1.40	d^{-1}
Maximum sinking rate of P	w_P	0.0448	m d^{-1}
Maximum sinking rate of Z	w_Z	0.0	m d^{-1}
Relative encounter velocity	U	310	μm s^{-1}

[a]Parameter values calculated from allometric relationships of *Baird et al.* [2004] for a 1 μm radius phytoplankton cell and 20 μm radius zooplankton cell.

waters off south east Australia by *Baird et al.* [2006a, 2006b]. In particular, the calculation of k_N, k_I and ϕ in terms of properties of the individual cells and environmental conditions is given by *Baird et al.* [2004]. The parameter values used in the simulations are summarized in Table 1 and are sourced from *Baird et al.* [2006a] and *Baird et al.* [2004], with the linear mortality rate of zooplankton, ζ_Z, being the only parameter whose value is changed.

2.3. Biological Model Initialization

[16] Initial conditions were determined using a similar long-duration spin-up to that used by *Baird et al.* [2004], the only adjustment being in using initial nutrient concentrations typical of the region. The spin-up consisted of a two-dimensional grid with zero-mean oscillating alongshore wind stress which sets up a realistic profile of vertical diffusivity. In particular, the idealized forcing forms a surface mixed layer. By oscillating between an upwelling and downwelling favorable wind stress, no net upwelling occurs. The two-dimensional model is run for 375 days, at which stage the time derivatives of the biological fields are small. The output from the two-dimensional grid after 375 days can be viewed as a quasi steady state response to idealized vertical mixing. A depth profile of the state variables at the center of the grid is then linearly interpolated onto the 3D Chilean grid to give the initial conditions. The biological model remained at initial conditions for the first 4 days of the simulation. This is necessary to avoid unrealistic vertical mixing of the initial vertical profile of the biological state variables during the physical model spin-up.

[17] The biological boundary conditions at the surface, bottom and coast (eastern boundary) are zero flux. The open boundaries (north, south and west) have a radiation condition and are relaxed to the quasi steady state initial conditions.

[18] The solar radiation flux, including a day-night cycle, and the zenith angle are calculated using orbital cycles [*Brock*, 1981], and the water surface albedo using Fresnel's equation [*Kirk*, 1994]. Snell's law is used to account for the refraction of light at the air/water interface [*Kirk*, 1994]. In order to exclude a seasonal signal and the small latitudinal variation, the whole model domain is forced with a solar radiation flux for January 1 at 36°S each model day.

2.4. Diagnostic Age Variable

[19] A diagnostic variable 'ideal age' [*England*, 1995; *Hall and Haine*, 2002] is used to track the transport of nutrient rich bottom waters. The dynamics of ideal age, τ, are described by

$$\frac{\partial \tau}{\partial t} + \mathbf{v} \cdot \nabla \tau = \nabla \cdot (K \nabla \tau) + \Theta(z), \tag{8}$$

where the symbol $\nabla = (\frac{\partial}{\partial x}, \frac{\partial}{\partial y}, \frac{\partial}{\partial z})$, $\mathbf{v}$ is the velocity field, K is the eddy diffusion coefficient which varies in space and time, and Θ is the local transformation of τ. Two forms of τ are considered, with the respective local transformation of

$$\tau_{90} : \Theta_{90}(z \leq 90 \text{ m depth}) = 1, \Theta_{90}(z > 90 \text{ m depth}) = 0 \tag{9}$$

$$\tau_{eu} : \Theta_{eu}\left(I \geq 0.01 I_{surface}\right) = 1, \Theta_{eu}\left(I < 0.01 I_{surface}\right) = 0. \tag{10}$$

The term Θ increments the value of τ by 1 day every day when the respective criterion are met. In order that Θ_{eu} increments at night as well as during the day, a negligible (but nonzero) surface nighttime irradiance is applied. Age in this application is the average time parcels of water within a volume have been above the 90 m depth level or the euphotic depth, respectively, since the biological state variables start varying. Age is subject to the same mixing and advective processes as the physical and biological tracers. The boundary conditions at the surface, bottom and coast for age are zero flux. On the open boundaries both τ_{eu} and τ_{90} are relaxed to zero below 90 m, and to the time

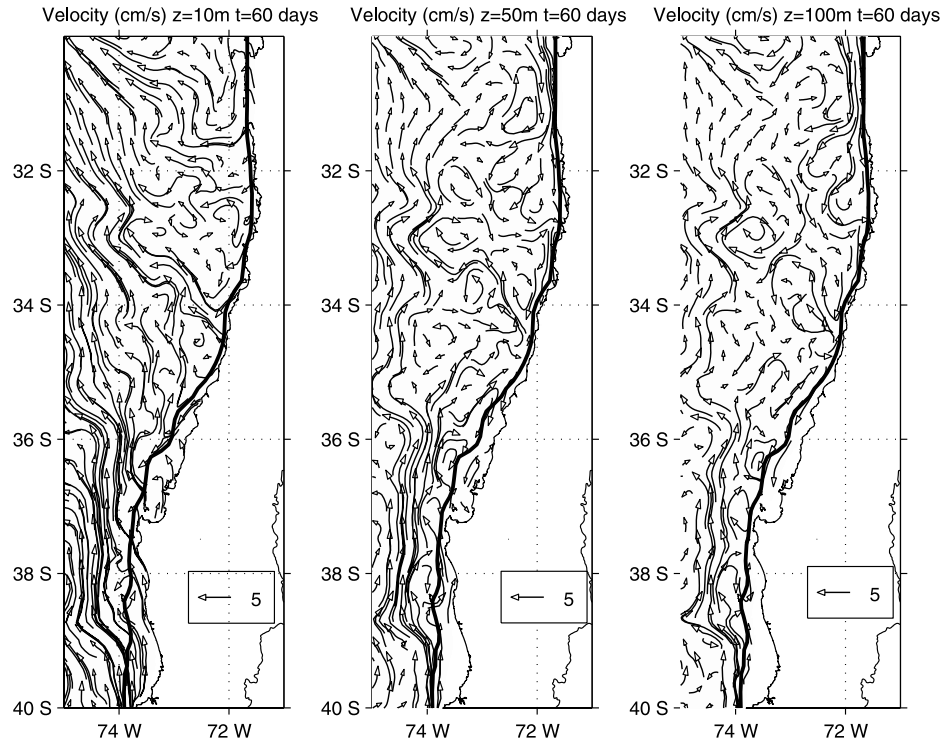

Figure 3. Horizontal velocity (cm s^{-1}) at (left) 10 m, (middle) 50 m, and (right) 100 m depth on day 60. The 200-m isobath is shown as a thick line, and the Chilean coast is shown as a thin line.

since the biological variables began varying in the top 90 m of the boundary.

3. Results

[21] Model time begins when the physical variables start varying, which, for the purpose of calculating the daily-varying irradiance, is midnight local time. The biological processes begin 4 days later. Model outputs are averaged over an inertial period (= $|2\pi/f|$ = 0.8507 d) where $f = -8.549 \times 10^{-5}$ s^{-1} is the Coriolis parameter at 36°S. That is, the output on day x is the mean of the output from $x - 0.4254$ to $x + 0.4254$. The diagnostic variable age is based on its instantaneous value.

3.1. Physical Model Behavior

[22] The currents at day 60 and at depths of 10 m, 50 m and 100 m are shown in Figure 3. In addition to cross shelf fluxes, there is often a strong component of along shelf flow, particular south of 38°S. The surface waters north of 38°S have a significant offshore component. At 50 m and 100 m, flow varies between on and off shelf, depending on the position of the eddies overlying the 200-m isobath. The net flow at depth is onshelf.

[23] Age, τ_{90}, is the average time parcels of water within a volume have been above the 90 m depth level since the beginning of the simulation. Surface waters that have little exchange with nutrient-rich bottom waters will have an age at time t of approximately $t - 4$ days, the four accounting for the initial spin-up time of the physical model before the age tracer is released. Figure 4 gives the age contours for two cross-shelf slices on days 40 and 60. The offshore surface waters in both slices approach an age older than 30 and 50 for model days 40 and 60 respectively, suggesting little vertical transport. In these offshore areas, τ_{90} depends on how long the simulation has been running. In contrast, the τ_{90} contours on days 40 and 60 in coastal regions generally overlie each other (Figure 4). Such a steady state for τ_{90} suggests that advection and vertical diffusion of young bottom waters is balancing the local aging of the water. This steady state is evidence of a relatively stable rate of upwelling between days 40 and 60.

3.2. NPZ Dynamics

[24] A surface view of the age (τ_{eu}), DIN, phytoplankton and zooplankton concentrations on days 36, 48 and 60 for the simulation with a linear zooplankton mortality coefficient, ζ_Z, equal to $0.25\mu_Z^{max}$ (or 0.35 d^{-1}) is given in Figure 5. A vertical cross-shelf slice intercepting the coast at 37°58′S is given in Figure 6. As mentioned above, age appears to have reached a steady state near the coast between days 40 to 60. This is evident in the similar surface patterns of age at day 48 and day 60 (Figures 5b and 5c) and in vertical sections (Figures 6b and 6c). Nonetheless, some non-steady state behavior remains, as illustrated by the lifting of the age contours by ~10 m at 74 W on day 60 (Figure 6c) compared to day 48 (Figure 6b).

[25] The upwelling at the coast is spatially variable. Filaments of young water are advected off the coast producing a jagged offshore front of upwelled water (Figures 5b and 5c). Along the coastline off Punta Lavapie (Figures 5b and 5c inserts) the 10 day age contour varies

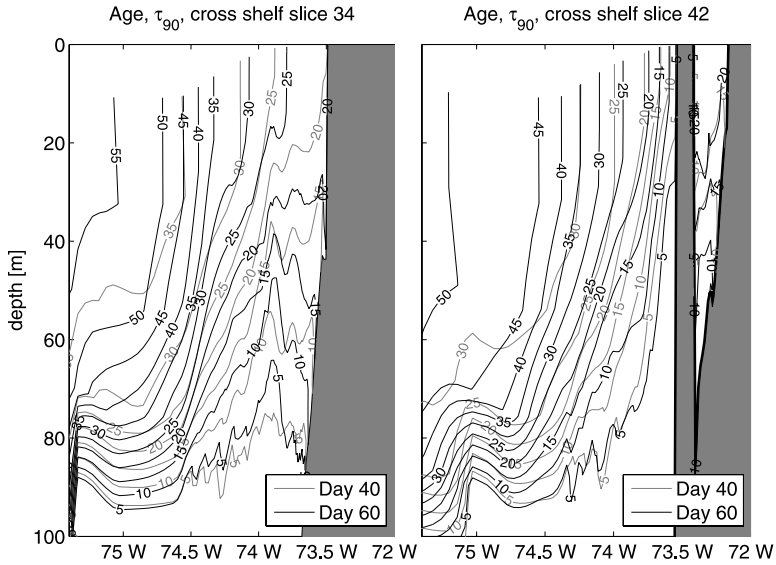

Figure 4. Model cross-shelf slices (left) 34 and (right) 42 of the diagnostic tracer age, τ_{90}, on day 40 (grey) and day 60 (black). Slice 34 intercepts the coast at 37°58′S, and slice 42 off Punta Lavapie at 37°00′S.

between a few and tens of kilometers offshore, while the 5 day contour intersects the coastline.

[26] The biological response to the coastal upwelling is characterized by high DIN concentration at the upwelling site (Figures 5d, 5e, 5f, 6d, 6e, and 6f), particularly for water less than 5 days old (inserts of Figures 5a, 5b, and 5c). As the water moves away from the upwelling site, DIN concentrations are depleted, and a phytoplankton bloom emerges (Figures 5g, 5h, 5i, 6g, 6h, and 6i). Farther downstream, phytoplankton concentration is depleted and a zooplankton maximum is evident (Figures 5j, 5k, 5l, 6j, 6k, and 6l).

[27] The biological state variables along the vertical slice intercepting the coast at 37°58′S at the same time points are shown in Figure 6. The vertical slice of age (Figures 6a–c), like Figure 4, shows that the upwelling system has reached a quasi-stable upwelling state. The biological state variables, in contrast, are still adjusting to the upwelling. From day 36 to 60 a phytoplankton bloom develops close to the coast (within ~10 km), drawing nutrients from the water column. From day 36 to 60 surface water is advected offshore, moving the phytoplankton front and DIN depletion front offshore. A zooplankton front forms downstream of the phytoplankton front, and is also being advected offshore (Figures 6g–6i). Additionally, local biological interactions generate noise, as illustrated later (section 3.5) by the existence of three phytoplankton productivity peaks on day 60.

[28] Phytoplankton and zooplankton response varies along the coast. At approximately 34°S on day 60 a filament of young water is advected northwest from the coast (Figure 5c). Along this filament phytoplankton biomass remains low (Figure 5i), while zooplankton biomass reaches it greatest concentrations (Figure 5l). At 36°S phytoplankton biomass escapes grazing control, and reaches it highest levels near the coast (Figure 5i), only to be consumed by zooplankton farther offshore, in a similar pattern to shown in the vertical slice at 37°58′S (Figure 6).

3.3. Sensitivity to the Linear Zooplankton Mortality Rate

[29] The zooplankton linear mortality coefficient, ζ_Z, represents loss of zooplankton to higher up the food chain or to dissolved inorganic nitrogen. While a number of higher-order closure terms are possible [*Edwards and Yool*, 2000], we have chosen a linear term for simplicity. We have determined the value of ζ_Z as a fraction of the maximum growth rate of zooplankton, $\mu_Z^{\max}$. As such, the change in zooplankton biomass due to biological processes can achieve a maximum rate of $(\mu_Z^{\max} - \zeta_Z)\, Z$.

[30] In the absence of zooplankton, phytoplankton could utilize all the DIN that is upwelled. The value of DIN at depth is 25 mmol N m^{-3}, of which in the model up to half may be stored as internal reserves (R_N), depending on whether growth is light or nutrient limited. Full utilization of DIN would represent a surface chlorophyll concentration of between 52 and 105 mg Chl *a* m^{-3} (for conversion factor see Table 1).

[31] To assess the impact of the zooplankton mortality term, simulations are run with ζ_Z equal to $0.125\mu_Z^{\max}$, $0.25\mu_Z^{\max}$ and $0.5\mu_Z^{\max}$ (corresponding to 0.175, 0.35 and 0.7 d^{-1}). For a value of $\zeta_Z = 0.5\mu_Z^{\max}$ the loss terms for zooplankton are high and the phytoplankton population is able to escape grazing control (Figure 7f), depleting DIN in the coastal regions (Figure 7c). Surprisingly, with high primary productivity zooplankton biomass is able to reach a relatively high biomass despite the strong loss term (Figure 7i).

[32] In contrast for a value of $\zeta_Z = 0.125\mu_Z^{\max}$ the loss terms for zooplankton are low and tight grazing control of the phytoplankton population is maintained (Figure 7d). With a low biomass, primary productivity is low, and the zooplankton population does not reach high levels

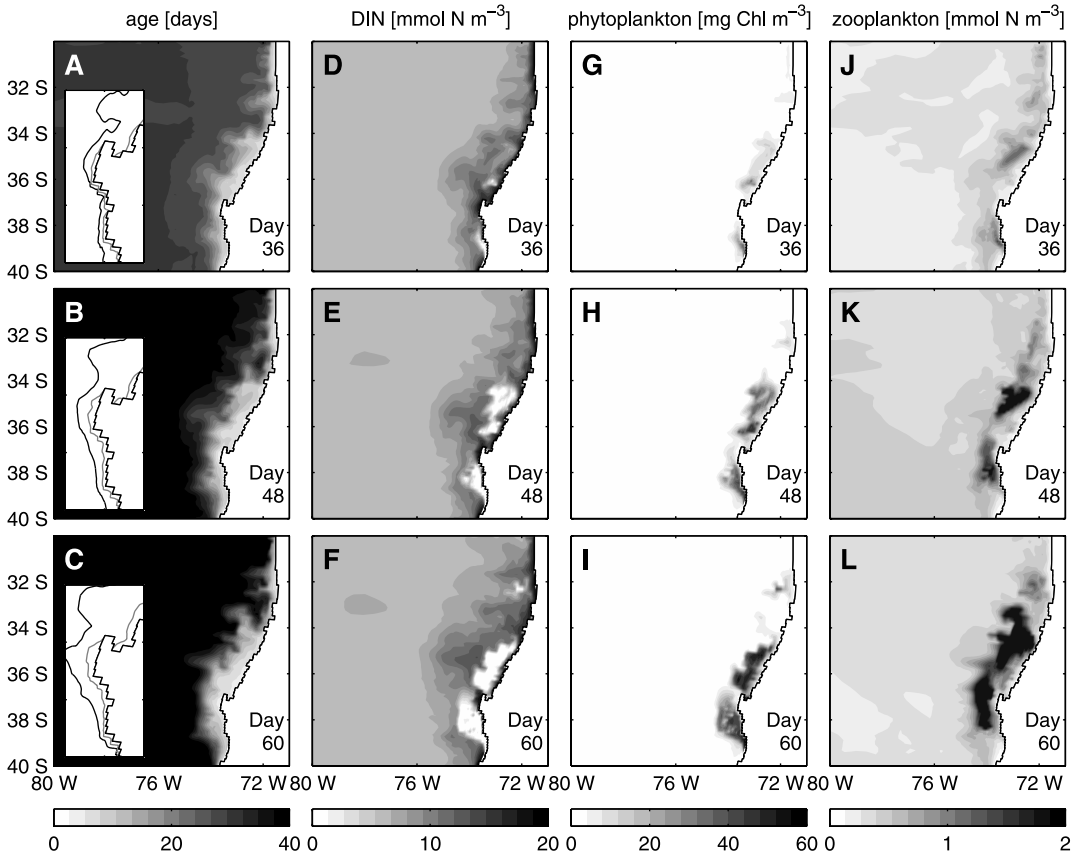

Figure 5. Age, τ_{eu}, dissolved inorganic nitrogen (DIN), phytoplankton, and zooplankton biomass on days 36, 48, and 60 of the $\zeta_Z = 0.25\ \mu_Z^{max}$ simulation interpolated on to a 10-m-depth level. The insert in Figures 5a, 5b, and 5c show the 5-day (gray) and 10-day (black) age contours offshore of Punta Lavapie on days 36, 48, and 60, respectively.

(Figure 7g), and the upwelled DIN is not fully utilized (Figure 7a). Interestingly, the effect of changing ζ_Z is spatially variable. In particular, doubling ζ_Z from $0.25\mu_Z^{max}$ to $0.5\mu_Z^{max}$ greatly increased the phytoplankton biomass north of 35°S, and offshore of Punta Lavapie (Figure 7f). In contrast, in regions with already high phytoplankton biomass (north and south of Punta Lavapie), the increases is less dramatic.

[33] On the basis of observations of primary productivity and chlorophyll concentration [*Cuevas et al.*, 2004] discussed below, a value of ζ_Z of between 0.125 μ_Z^{max} and 0.25 μ_Z^{max} (or 0.175–0.35 d^{-1}) probably best captures the dynamics between phytoplankton, zooplankton, and zooplankton loss processes. In the next section the implications of changing grazing pressure for biogeochemical budgets is considered.

3.4. Model Biogeochemical Fluxes on the Continental Shelf

[34] The Chilean coast has a narrow, but highly productive, continental shelf. In the model, the continental shelf, defined by the 200 m depth contour, extends for 1500 km, and has an area of 35.65×10^3 km^2. The budgets for nitrogen on the continental shelf for day 60 of the ζ_Z equal to 0.5 μ_Z^{max}, 0.25 μ_Z^{max} and 0.125 μ_Z^{max} simulations are shown in Figures 8a–8c. The small discrepancies in the budgets are due to fluxes on the continental shelf from the north and south, and rounding errors.

[35] The budgets for ζ_Z equal to 0.5 μ_Z^{max} and 0.25 μ_Z^{max} are similar. For ζ_Z equal to 0.5 μ_Z^{max} (Figure 8a), 80% of the nitrogen on the shelf is DIN, with 19% phytoplankton biomass and 1% zooplankton biomass. Integrated over the whole shelf, 27 Gg N d^{-1} of DIN is brought onto the shelf, with 30 and 1 Gg N d^{-1} of phytoplankton and zooplankton respectively being exported off. The gross primary productivity along the whole shelf is 76 Gg N d^{-1}, or 11 g C m^{-2} d^{-1}. This value appears high compared to measured values of between 0.3 and 9.6 g C m^{-2} d^{-1} [*Cuevas et al.*, 2004; *Fossing et al.*, 1995].

[36] The gross primary productivity for the ζ_Z equal to 0.125 μ_Z^{max} case (Figure 8c) is 4.9 g C m^{-2} d^{-1}. Under this case, with tight grazing control of phytoplankton due to a low zooplankton mortality, phytoplankton biomass remains low, and the export of organic matter off the shelf is reduced.

[37] To obtain a spatially resolved picture of across shelf fluxes, the continental shelf boundary is defined by the eastern most cell along each east-west slice with a depth greater than 200 m. The average depth of these cells is 214 m, with a range between 201 and 254 m. Faces are created by joining these points in the horizontal, and using the sigma levels at each point to define the vertical extent of the face.

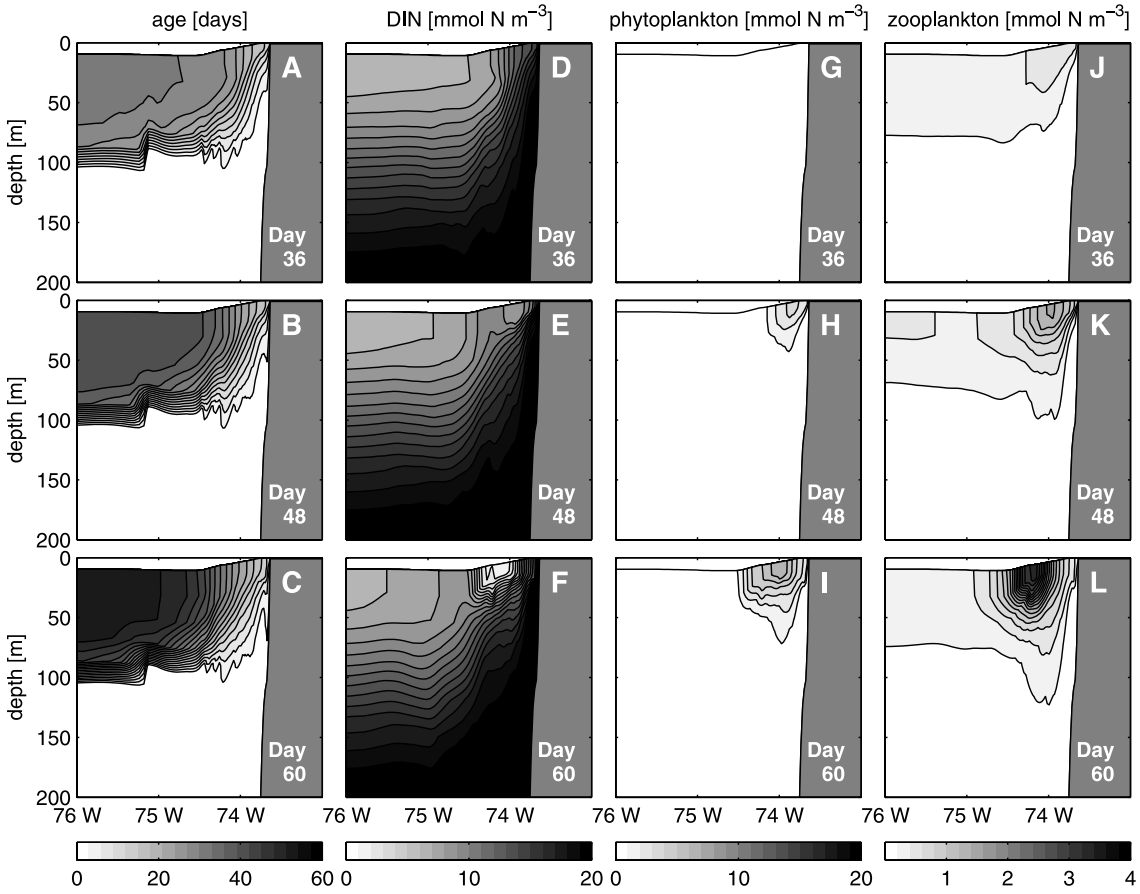

Figure 6. Age, τ_{eu}, dissolved inorganic nitrogen (DIN), phytoplankton, and zooplankton biomass on days 36, 48, and 60 of the $\zeta_Z = 0.25\ \mu_Z^{\max}$ simulation on the cross-shelf model slice 34, which intercepts the coast at 37°58′S.

The flux across these faces is then calculated on the basis of the u and v components of the model velocity across the faces of the model grid. The net across shelf flux of water of −0.9 Sv on day 60 is the difference between the specified transports at the northern and southern open boundaries for water shallower than 200 m (Figure 1 gives the open boundary conditions). On day 60, the net flux is composed of a flux of 3.7 Sv on shelf, and 4.6 Sv off shelf. The spatial distribution of the cross shelf flux of water on day 60 is shown in Figure 9a. In the top 20 m, water is primarily moving offshore, with the exception of a vertical column of onshore transport just south of Punta Lavapie (38°S). Below 20 m depth, both onshore and offshore movement is seen.

[38] The fluxes of organic nitrogen (sum of total phytoplankton nitrogen and zooplankton nitrogen) are identical in direction to the water (Figures 9b–9d). The major difference in magnitude between water and organic nitrogen fluxes is the greater surface flux of organic nitrogen relative to that at depth, a result of the production of organic nitrogen from dissolved inorganic nitrogen through photosynthesis on the continental shelf.

[39] The differences between simulations with varying values of ζ_Z are evident in the continental shelf flux of organic nitrogen (Figures 9b–9d). The ζ_Z equal to $0.125\ \mu_Z^{\max}$ case has a much smaller surface organic nitrogen flux than the $0.25\ \mu_Z^{\max}$ and $0.5\ \mu_Z^{\max}$ cases. Additionally, the $0.25\ \mu_Z^{\max}$ and $0.5\ \mu_Z^{\max}$ cases have greater offshore flux in the northern sections of the shelf, a result of higher biomass (compare Figure 7f with Figure 7d). In all three cases there is little export across the 200-m isobath directly off Punta Lavapie. This occurs because flow is generally alongshore and the biomass of phytoplankton and zooplankton is low owing to the short duration since the water was below the euphotic zone (Figures 5c, 5f, 5i, and 5l).

3.5. Phytoplankton and Zooplankton Productivity

[40] The surface phytoplankton dynamical terms at day 60 of the ζ_Z equal to $0.25\ \mu_Z^{\max}$ simulation reveal the processes determining the spatial distribution of the phytoplankton biomass (Figure 10). Phytoplankton tendency is generally positive close to the coast (Figure 10a), particularly north and south of Punta Lavapie (37°S) owing to strong growth (Figure 10d). In fact, close to the coast, advection (of low phytoplankton concentration waters from below) is a significant negative term (Figure 10b). At the surface, vertical diffusion is generally a negative term, diluting phytoplankton with waters from below the mixed layer (Figure 10c). The small regions of a positive vertical diffusion for phytoplankton represent areas where the phy-

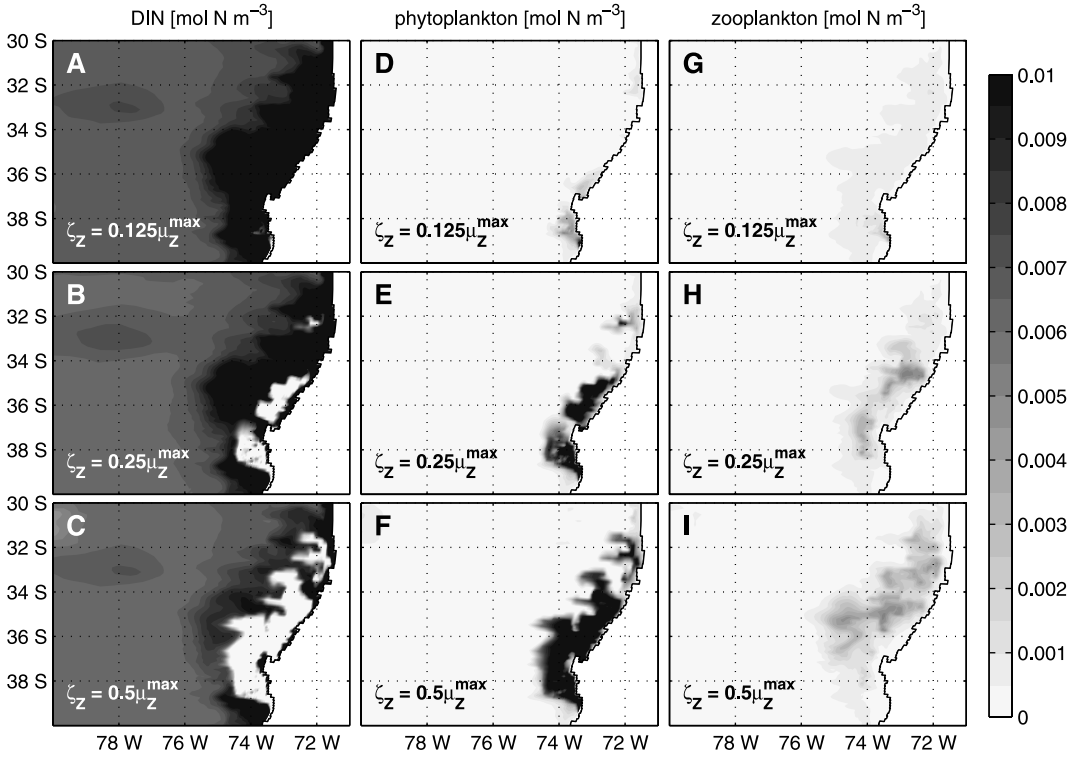

Figure 7. Dissolved inorganic nitrogen (DIN), phytoplankton, and zooplankton biomass for the simulations with ζ_Z equal to (top) 0.125 μ_Z^{max}, (middle) 0.25 μ_Z^{max}, and (bottom) 0.5 μ_Z^{max} interpolated on to a 10-m-depth surface on day 60.

toplankton biomass has a maximum biomass below the surface.

[41] Farther offshore, where zooplankton biomass is greater, grazing becomes an important loss term (Figure 10e), becoming greater than growth (Figure 10d), resulting in a negative tendency (Figure 10a). At this distance offshore advection becomes a positive term (Figure 10b), a result of the advection of high phytoplankton biomass waters into regions being strongly depleted by grazing.

[42] Another view of phytoplankton dynamics can be obtained with depth integration of the biomass (Figure 11a) and primary productivity (Figure 11b). For comparison with observations [*Cuevas et al.*, 2004], the depth of integration chosen is the euphotic depth. Depth-integrated phytoplankton

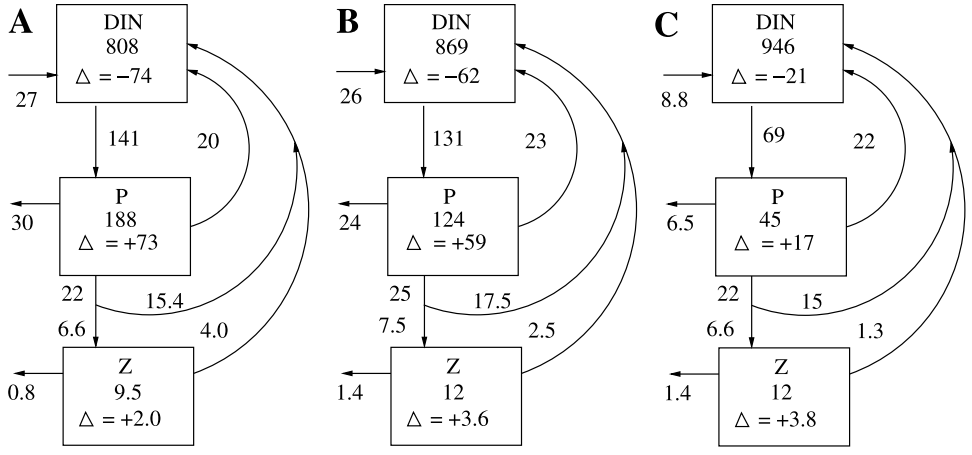

Figure 8. Nitrogen budget for the continental shelf on day 60 for ζ_Z equal to (a) 0.5 μ_Z^{max}, (b) 0.25 μ_Z^{max}, and (c) 0.125 μ_Z^{max}. The shelf is defined by the 200-m-depth contour. Concentration is in Gg N, and fluxes are in Gg N d^{-1}. The phytoplankton biomass and phytoplankton terms are based on total algal nitrogen, or $(1 + R_N/R_N^{max})$ *P*. Arrows to the left of each box represent fluxes across the 200-m isobath. The up-pointing triangle represents the local rate of change or tendency.

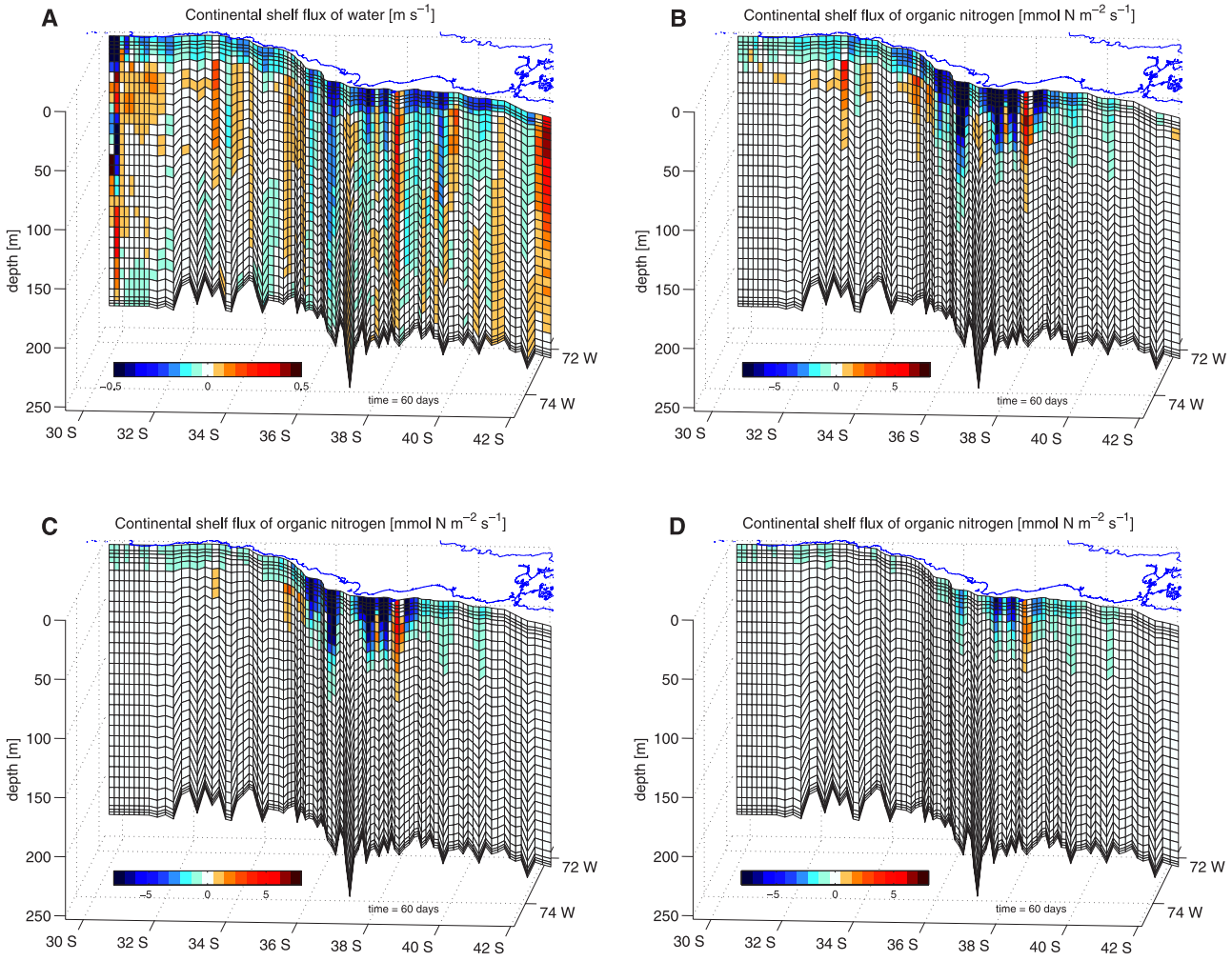

Figure 9. Flux of (a) water and organic nitrogen for ζ_Z equal to (b) 0.5 μ_Z^{max}, (c) 0.25 μ_Z^{max}, and (d) 0.125 μ_Z^{max} on day 60 between the continental shelf and the open ocean. Positive (red) is onto the continental shelf, negative (blue) is off the shelf, and white is zero flux. The blue line at depth zero shows the South American coastline. The edge of the continental shelf is defined by the first grid point greater than 200 m in depth in an offshore direction. The vertical curtain drops from the surface to the bottom, with the horizontal lines being determined by the vertical sigma coordinate system.

reaches its highest values farther offshore than the surface phytoplankton peak (Figure 5e), a result of the deepening of the surface mixed layer. Depth-integrated primary productivity (Figure 11b) has a similar spatial distribution to depth-integrated biomass (Figure 11a).

[43] The euphotic zone depth, Z_{eu}, is defined as the depth level at which solar radiation is 1% of the surface value. In regions well offshore, Z_{eu} is approximately 70 m, shallowing close to the coast (Figure 11c) owing to absorption by phytoplankton cells. In shallow depths close to the coast the euphotic zone reaches the bottom.

[44] A scatter plot of primary productivity versus depth-integrated chlorophyll (Figure 11d) shows that phytoplankton is growing at between 40% and 90% of the maximum growth rate. The exception is a cluster of points at high depth-integrated phytoplankton biomass with a shallow euphotic zone. These columns of water are generally young water (Figure 11e) that are depleted in dissolved nitrogen (Figure 11f). A combination of light limitation and nutrient limitation keeps growth rate in these high depth-integrated chlorophyll and shallow euphotic depth regions low. The populations growing closest to the maximum growth rate are generally either old with very low biomass (as shown by a line of dark grey dots closest to the upper line in Figure 11e) or young with high DIN concentrations (dark grey dots closest to the upper line in Figure 11f). The remaining areas are characteristically well offshore, with a deep euphotic depth, and are growing at between 40% and 80% of the maximum growth rate.

[45] The surface zooplankton dynamical terms at day 60 of the ζ_Z equal to 0.25 μ_Z^{max} simulation are similar to the phytoplankton dynamical terms (Figure 12). The major difference is zooplankton production (Figure 12d) is found farther offshore.

[46] A vertical slice of the phytoplankton and zooplankton production terms on days 36, 48 and 60 (Figure 13) shows the movement of the production fronts offshore. The phytoplankton production has reached a maximum by

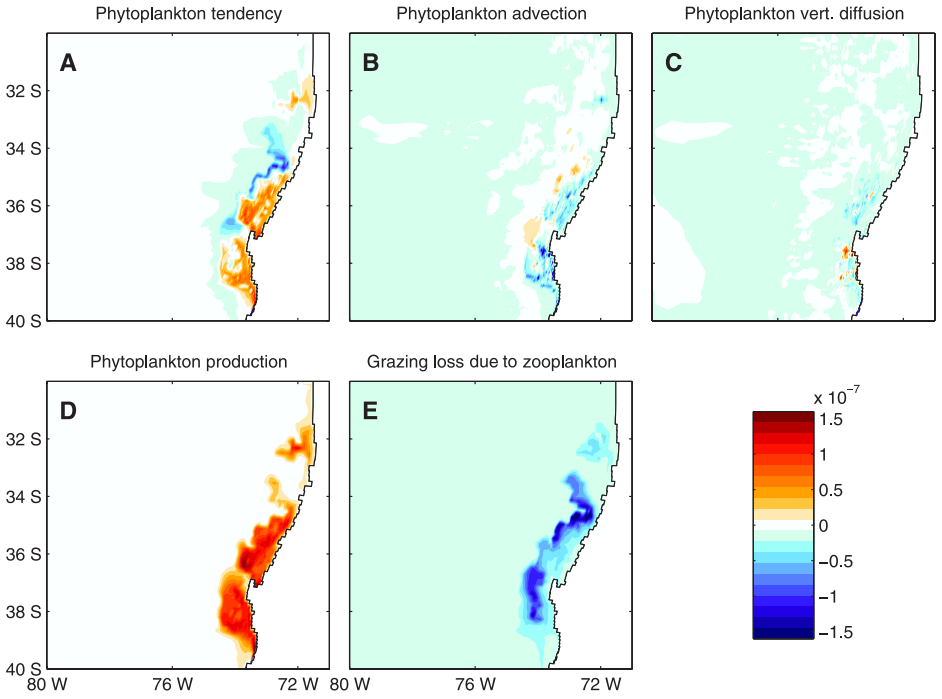

Figure 10. Phytoplankton terms [mol N m^{-3} s^{-1}] for the $\zeta_Z = 0.25\ \mu_Z^{max}$ simulation interpolated onto a 10-m-depth surface on day 60. (a) Tendency, the local rate of change, given by the sum of all other terms, (b) advection (both horizontal and vertical) as resolved by the positive definite advection scheme [*Smolarkiewicz*, 1984] that includes an antidiffusion term, (c) vertical diffusion as solved by the *Mellor and Yamada* [1982] turbulence closure scheme, (d) phytoplankton production, and (e) grazing loss due to zooplankton. Positive (red) is a gain in phytoplankton, negative (blue) is a loss, and white is zero.

day 48, and extends in area for the next 12 days, while the zooplankton production maximum is both extending in area and increasing in magnitude. Zooplankton productivity reaches deeper into the water column, primarily owing to the greater depth of the mixed layer offshore where the maximum zooplankton biomass occurs. A secondary factor is the light limitation of growth at depth due to shelf-shading.

3.6. Timing of the Biological Response

[47] The timing of the biological response along the Chilean coast of the ζ_Z equal to 0.25 μ_Z^{max} simulation is investigated using the diagnostic tracer age (for a description see section 2.4). For the purposes of investigating biological behavior, we will use τ_{eu}, which ages according to whether the water is within the euphotic zone.

[48] The initial total biomass of nitrogen is ~7 mmol N m^{-3} in the surface, linearly increasing to ~25 mmol N m^{-3} below 400 m. Mixing of deep and surface waters approximates a mixing line between total nitrogen and age (Figure 14d). For waters more than 40 days old, mixing with deep water is slow, and the DIN, phytoplankton and zooplankton concentrations adjust relatively smoothly to changes in total nitrogen (Figures 14a–14c). These waters are already close to a steady state as a result of the initializing of the biological state variables with output from a 375 day spin-up. For water less than 40 days old, some of the points show large deviations from the mixing line for DIN, a result of quick changes in environmental forcing (i.e., changing light climate in upwelled water) taking the biological variables away from a steady state.

[49] On day 60 the youngest water at the surface is about 3 days old, representing the time required for water to be transported from below the euphotic zone to the surface (Figure 14). In the 3 day old water, the DIN concentration generally has its highest surface value, of approximately 0.022 mol N m^{-3} (Figure 14a). DIN concentration generally decreases with τ_{eu} (Figure 14a). The points showing a rapid decreases in DIN with τ_{eu} (Figure 14a) are from coastal waters where there is strong DIN uptake.

[50] The phytoplankton biomass has a maximum in coastal waters for τ_{eu} between 5 and 15 days (Figure 14b). The zooplankton biomass has a maximum offshore of the phytoplankton maximum, at τ_{eu} of between 10 and 25 days (Figure 14c). Phytoplankton blooms last approximately 20 days. Lines can be seen on the scatter plot where filaments of water are sufficiently coherent that distance along a filament corresponds to time in the euphotic zone, τ_{eu} [*Baird et al.*, 2004].

[51] The timing of the chlorophyll maximum can be compared to observed chlorophyll filaments off the Chilean coast. *Marín et al.* [2003] analyzed filaments on the 20 January 1999 and 19 January 2002 at 30°S (on the northern edge of the model domain) with delimiting chlorophyll concentrations of 0.7 and 0.5 mg m^{-3} respectively. The limit of the filaments were observed 141 and 125 km along the main axis of the filament. With velocities of between 0.1 and 0.2 m s^{-1} at the front edge of the filament,

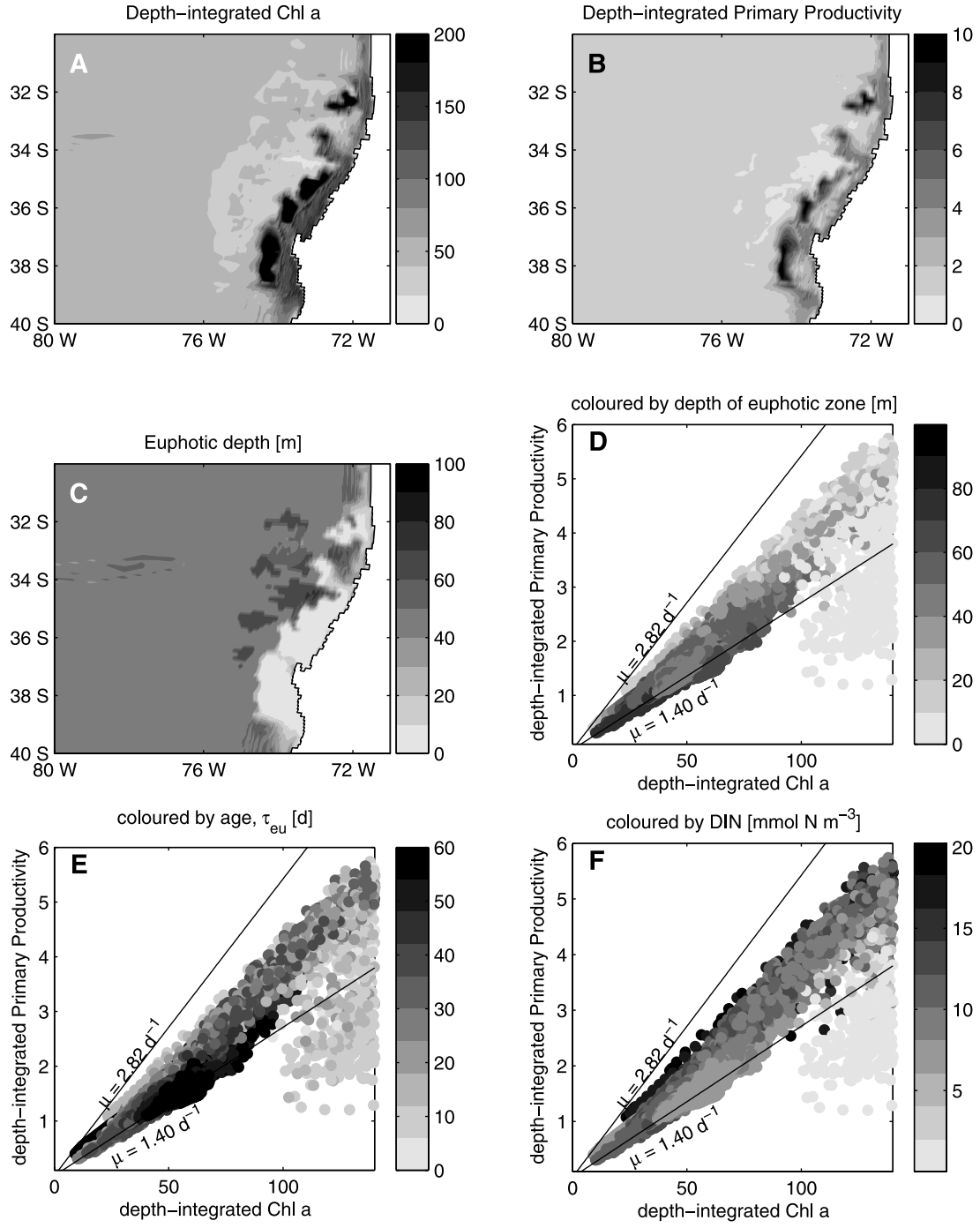

Figure 11. (a) Depth-integrated Chl *a* (mg Chl *a* m^{-2}), (b) depth-integrated primary productivity (g C m^{-2} d^{-1}), (c) depth of the euphotic zone (defined by $I_{eu} = 0.01 I_{surface}$), and depth-integrated Chl *a* versus depth-integrated primary productivity, colored by (d) euphotic depth (meters), (e) surface age, τ_{eu} (days), and (f) surface dissolved inorganic nitrogen (mmol N m^{-3}) for $\zeta_Z = 0.25\ \mu_Z^{\max}$ on day 60. The depth of integration was taken to be the euphotic depth.

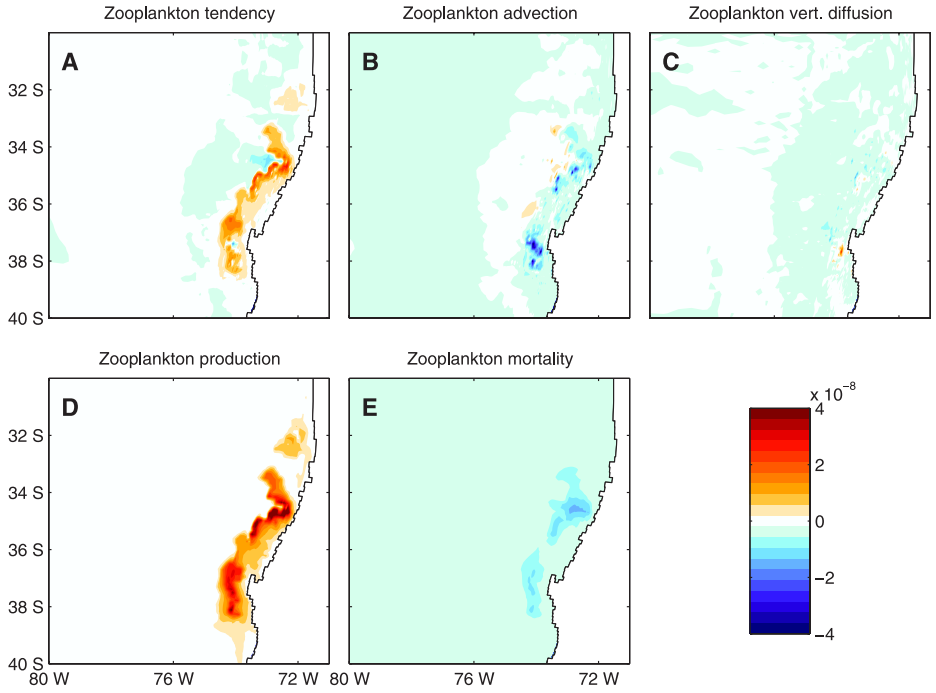

Figure 12. Zooplankton terms (mol N m^{-3} s^{-1}) for the $\zeta_Z = 0.25\ \mu_Z^{max}$ simulation interpolated onto a 10-m-depth surface on day 60. (a) Tendency, the local rate of change, given by the sum of all other terms, (b) advection (both horizontal and vertical) as resolved by the positive definite advection scheme [*Smolarkiewicz*, 1984] that includes an antidiffusion term, (c) vertical diffusion as solved by the *Mellor and Yamada* [1982] turbulence closure scheme, (d) zooplankton production, and (e) mortality of zooplankton. Positive (red) is a gain in zooplankton, negative (blue) is a loss, and white is zero.

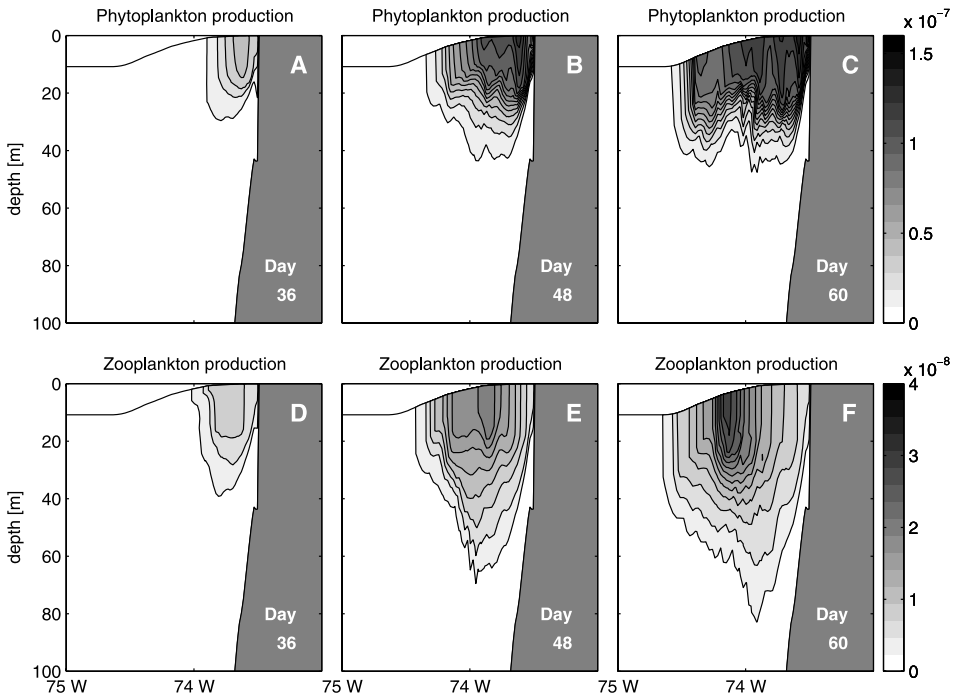

Figure 13. Phytoplankton and zooplankton production (mol N m^{-3} s^{-1}) for the $\zeta_Z = 0.25\ \mu_Z^{max}$ simulation on days 36, 48, and 60 along cross-shelf model slice 34, which intercepts the coast at 37°58′S.

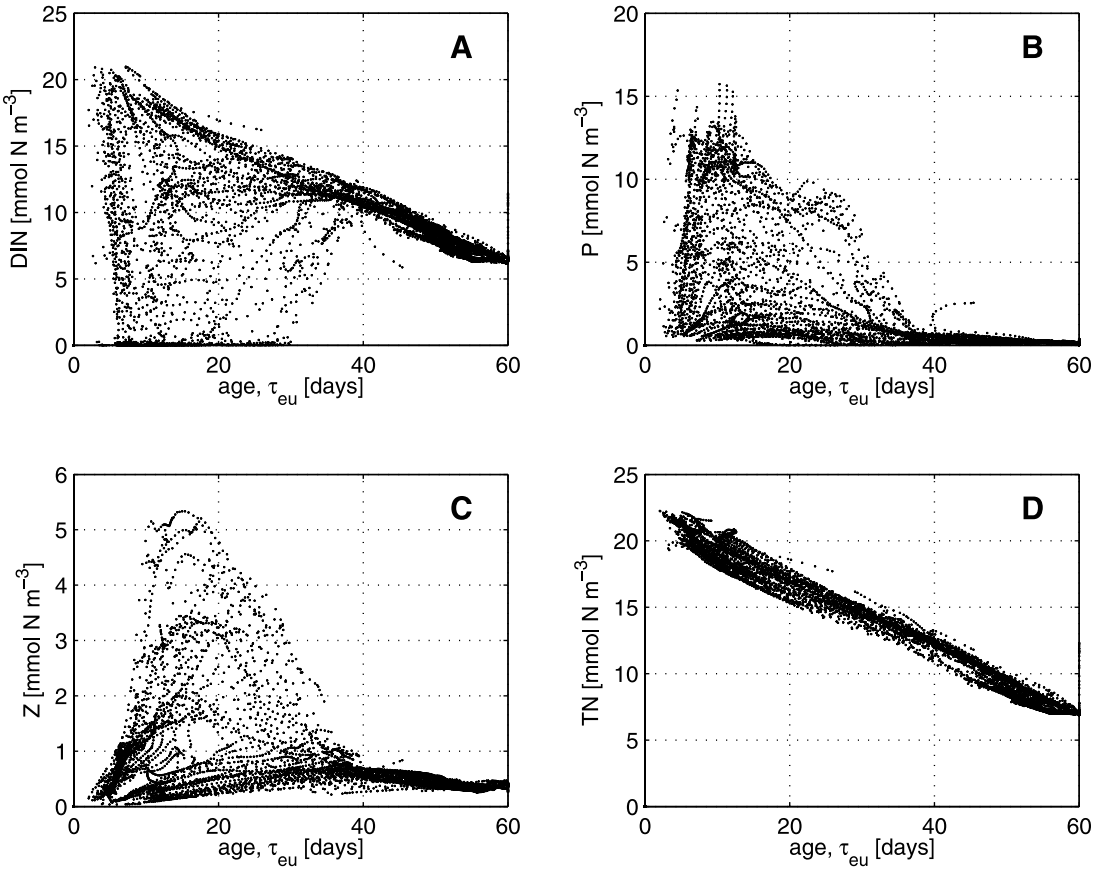

Figure 14. Phase space plots at the surface (interpolated from the σ-grid onto a 10-m z-level) of (a) DIN, (b) phytoplankton biomass, (c) zooplankton biomass, and (d) total nitrogen against age, τ_{eu}, for day 60 of the $\zeta_Z = 0.25\ \mu_Z^{\max}$ simulation.

this represents an age (since reaching the surface) of between 16 and 29 days. which is of the same order as the demise of the phytoplankton biomass in Figure 14b.

3.7. Discussion and Summary

[52] The central Chilean upwelling system is one of the most productive in the world [*Daneri et al.*, 2000]. The major fisheries of the region are considered to be at a trophic level of approximately 3 [*Neira and Arancibia*, 2004]. This third trophic level is not resolved in the biological model, but its effect is represented by the linear mortality term on the zooplankton. A simplified view of the system would equate variations in ζ_Z with changing fish stocks due to natural variability and/or fishing pressure. While the natural system is likely to be much more complex than this simple representation, the simulations illustrate a potential effect of variability in fish stocks on the biomass of lower trophic levels, and on fluxes of organic matter between the continental shelf and deep ocean.

[53] The idealized nature of the physical model forcing, and the simplicity of the biological model, sets limits to the details of the model which can be compared with field data. The alongshore resolution of ~15 km is insufficient to resolve a number of important topographic and bathymetric features, including the Biobio submarine canyon that is known to produce significant upwelling [*Sobarzo et al.*, 2001; *Hernandez et al.*, 2006]. The use of a constant mean summertime wind-stress field will smooth episodic upwelling events when compared to forcing with a real wind-stress field. The effect of large river flows such as the Rio BioBio on density, nutrient inputs and vertical attenuation may also be important. While this paper explored the impact of the mortality of zooplankton on model dynamics, a more detailed effort to calculate this term, perhaps through a multiple size-class biological model, would be useful.

[54] The importance of zooplankton parameterization in determining the spatial and temporal dynamics of phytoplankton and zooplankton has been shown for upwelling conditions off the Oregon coast [*Spitz et al.*, 2003]. *Spitz et al.* [2003] found that increasing the maximum grazing rate of zooplankton on phytoplankton restricted the phytoplankton blooms to the coast, and resulted in a more intense zooplankton maximum just offshore of the phytoplankton bloom (compare Figures 17 and 19 of *Spitz et al.* [2003]). The high maximum grazing rate case of *Spitz et al.* [2003] is similar to the low zooplankton mortality case ($0.125\ \mu_Z^{\max}$) in this paper. In both studies, zooplankton control of phytoplankton biomass restricts phytoplankton blooms to close to the coast. Similarly, the low maximum grazing rate case of *Spitz et al.* [2003] and the high zooplankton mortality case in this paper have larger phytoplankton blooms that reach farther offshore. The *Spitz et al.* [2003] manipulation of the maximum zooplankton grazing term provides an indication of the sensitivity of their model to the

interaction between phytoplankton and zooplankton, while the manipulation of the mortality rate of zooplankton in this study examines the sensitivity to interaction of zooplankton and their predators. It is clear both are important in predicting not only zooplankton dynamics, but also phytoplankton and nutrient dynamics.

[55] The model results published here are the first results from a nitrogen-phytoplankton-zooplankton model forced by a high-resolution hydrodynamical model for the waters off central Chile, and provide insights into the dynamics of one of the world's most biologically productive regions. The circulation driven by the mean summertime wind stress, combined with high nutrient concentrations at depth, is capable of producing extremely high Chl *a* values in coastal regions.

[56] The magnitude, and spatial distribution of Chl *a* that is realized depends strongly on the grazing pressure on zooplankton. Under high grazing pressure, zooplankton production is lower than phytoplankton production, and phytoplankton escape grazing control, resulting in high phytoplankton biomass and productivity in coastal regions, and significant export of organic matter from the continental shelf. Under low grazing pressure on zooplankton, phytoplankton biomass is tightly controlled, resulting in low primary productivity, and low zooplankton biomass. As a result, organic matter export off the shelf is greatly reduced. This illustrates the potential top-down control of the very productive waters off central Chile, and suggests variability in fish stocks may play a role in the biogeochemistry of the region.

[57] **Acknowledgments.** This research was funded by ARC Discovery Project DP0557618 held by M. B. We thank Alan Blumberg and George Mellor for the free availability of the Princeton Ocean Model, Peter Oke, Patrick Timko, Jason Middleton, and Iain Suthers for earlier work on the biological module, and the use of the Australian Partnership for Advanced Computing (APAC) supercomputer.

References

Atkinson, L. P., A. Valle-Levinson, D. Figueroa, R. D. Pol-Holz, V. A. Gallardo, W. Schneide, J. L. Blanco, and M. Schmidt (2002), Oceanographic observations in Chilean coastal waters between Valdivia and Concepcion, *J. Geophys. Res.*, *107*(C7), 3081, doi:10.1029/2001JC000991.

Baird, M. E., P. R. Oke, I. M. Suthers, and J. H. Middleton (2004), A plankton population model with bio-mechanical descriptions of biological processes in an idealised 2-D ocean basin, *J. Mar. Syst.*, *50*, 199–222.

Baird, M. E., P. G. Timko, I. M. Suthers, and J. H. Middleton (2006a), Coupled physical-biological modelling study of the East Australian Current with idealised wind forcing. Part I: Biological model intercomparison, *J. Mar. Syst.*, *59*, 249–270.

Baird, M. E., P. G. Timko, I. M. Suthers, and J. H. Middleton (2006b), Coupled physical-biological modelling study of the East Australian Current with idealised wind forcing: Part II: Biological dynamical analysis, *J. Mar. Syst.*, *59*, 271–291.

Blumberg, A. F., and G. L. Mellor (1987), A description of a three-dimensional coastal ocean circulation model, in *Three-Dimensional Coastal Ocean Models, Coastal Estuarine Stud.*, vol. 4, edited by N. Heaps, pp. 1–15, AGU, Washington, D. C.

Brock, T. D. (1981), Calculating solar radiation for ecological studies, *Ecol. Modell.*, *14*, 1–19.

Craig, P. D., and M. L. Banner (1994), Modeling wave-enhanced turbulence in the ocean surface layer, *J. Phys. Oceanogr.*, *24*, 2546–2559.

Cuevas, L. A., G. Daneri, B. Jacob, and P. Montero (2004), Microbial abundance and activity in the seasonal upwelling area off Concepción (~36°S), central Chile: A comparison of upwelling and non-upwelling conditions, *Deep Sea Res., Part II*, *51*, 2427–2440.

Daneri, G., V. Dellarossa, R. Qui, B. Jacob, P. Montero, and O. Ulloa (2000), Primary production and community respiration in the Humboldt Current System off Chile and associated areas, *Mar. Ecol. Prog. Ser.*, *197*, 41–49.

Edwards, A. M., and A. Yool (2000), The role of higher predation in plankton population models, *J. Plankton Res.*, *22*, 1085–1112.

England, M. H. (1995), The age of water and ventilation timescales in a global ocean model, *J. Phys. Oceanogr.*, *25*, 2756–2777.

Fossing, H., et al. (1995), Concentration and transport of nitrate by the mat-forming sulphur bacterium *Thioploca*, *Nature*, *374*, 713–715.

Hall, T. M., and T. W. N. Haine (2002), On ocean transport diagnostics: The idealized age tracer and the age spectrum, *J. Phys. Oceanogr.*, *32*, 1987–1991.

Hernandez, K. L., R. A. Quinones, G. Daneri, and E. W. Helbling (2006), Effects of solar radiation on bacterioplankton production in the upwelling system off central-southern Chile, *Mar. Ecol. Prog. Ser.*, *315*, 19–31.

Jackson, G. A. (1995), Coagulation of marine algae, in *Aquatic Chemistry: Interfacial and Interspecies Processes*, edited by C. P. Huang, C. R. O'Melia, and J. J. Morgan, pp. 203–217, Am. Chem. Soc., Washington, D. C.

Kirk, J. T. O. (1994), *Light and Photosynthesis in Aquatic Ecosystems*, 2nd ed., Cambridge Univ. Press, New York.

Leth, O., and J. F. Middleton (2004), A mechanism for enhanced upwelling off central Chile: Eddy advection, *J. Geophys. Res.*, *109*, C12020, doi:10.1029/2003JC002129.

Leth, O., and G. Shaffer (2001), A numerical study of the seasonal variability in the circulation off central Chile, *J. Geophys. Res.*, *106*(C10), 22,229–22,248.

Levitus, S., and T. P. Boyer (1994), *World Ocean Atlas 1994*, vol. 4, *Temperature*, *NOAA Atlas NESDIS*, vol. 4, 129 pp., NOAA, Silver Spring, Md.

Levitus, S., R. Burgett, and T. P. Boyer (1994), *World Ocean Atlas 1994*, vol. 3, *Salinity*, *NOAA Atlas NESDIS*, vol. 3, 111 pp., NOAA, Silver Spring, Md.

Marín, V. H., L. Delgado, and G. Luna-Jorquera (2003), S-chlorophyll squirts at 30°S off the Chilean coast (eastern South Pacific): Feature-tracking analysis, *J. Geophys. Res.*, *108*(C12), 3378, doi:10.1029/2003JC001935.

Mellor, G. L., and T. Yamada (1982), Development of a turbulent closure model for geophysical fluid problems, *Rev. Geophys.*, *20*, 851–875.

Mesias, J. M., R. P. Mantano, and P. T. Strub (2003), Dynamical analysis of the upwelling circulation off central Chile, *J. Geophys. Res.*, *108*(C3), 3085, doi:10.1029/2001JC001135.

Neira, S., and H. Arancibia (2004), Trophic interactions and community structure in the upwelling system off central Chile (33–39°S), *J. Exp. Mar. Biol. Ecol.*, *312*, 349–366.

Redfield, A. C., B. H. Ketchum, and F. A. Richards (1963), The influence of organisms on the composition of sea-water, in *The Sea*, 2nd ed., edited by N. Hill, pp. 26–77, John Wiley, Hoboken, N. J.

Smolarkiewicz, P. K. (1984), A fully multidimensional positive definite advection transport algorithm with small implicit diffusion, *J. Comput. Phys.*, *54*, 325–362.

Sobarzo, M., M. Figueroa, and L. Djurfeldt (2001), Upwelling of subsurface water into the rim of the Biobio submarine canyon as a response to surface winds, *Cont. Shelf Res.*, *21*, 279–299.

Spitz, Y., P. Newberger, and J. Allen (2003), Ecosystem response to upwelling off the Oregon coast: Behavior of three nitrogen-based models, *J. Geophys. Res.*, *108*(C3), 3062, doi:10.1029/2001JC001181.

M. E. Baird, Climate and Environmental Dynamics Laboratory, School of Mathematics and Statistics, University of New South Wales, Sydney, NSW 2052, Australia. (m.baird@unsw.edu.au)

O. Leth, Centre for Ocean and Ice, Danish Meteorological Institute, Lyngbyvej 100, DK-2100 Copenhagen, Denmark. (okl@dmi.dk)

J. F. Middleton, Aquatic Sciences, South Australian Research and Development Institute, P.O. Box 120, Henley Beach, SA 5022, Australia. (middleton.john@saugov.sa.gov.au)